Carbon Capture Science & Technology 6 (2023) 100096

Contents lists available at ScienceDirect

Carbon Capture Science & Technology

journal homepage: www.elsevier.com/locate/ccst

Full Length Article

Ageing study of Li-Ru/Al_2O_3 dual function material during the integrated CO_2 capture and methanation with SO_2-containing flue gas

Stefano Cimino*, Elisabetta Maria Cepollaro, Luciana Lisi

CNR-STEMS Science and Technology for Sustainable Energy and Mobility, Via G. Marconi 4, Napoli 80125, Italy

ARTICLE INFO

Keywords:
CO_2 Capture and Utilization
Power to Gas
Renewable Methane
Chemical Looping
Ruthenium
Sulfur Poisoning

ABSTRACT

A Dual Function Material containing Ru (1% wt.) and Li (3% wt.) dispersed by sequential impregnations onto Al_2O_3 spheres was extensively tested in the integrated CO_2 capture and methanation process to assess the effects of the main species (O_2 and H_2O) as well as of poisonous impurities (SO_2) in realistic flue gases. The DFM designed in this work was benchmarked against the state-of-the-art formulation (Ru and Na) in terms of intrinsic methanation activity as well as CO_2 capture capacity, CH_4 production and selectivity across more than 100 repeated cycles performed in a fixed bed reactor operated in the temperature range 260–320 °C with alternate feed conditions. The ageing study with up to 100ppmv SO_2 demonstrated a remarkable tolerance to sulfur poisoning coupled with a slow loss of CO_2 capacity due to long-term S-accumulation. A detailed characterization of the fresh and S-aged DFM was performed to get insights into mechanistic aspects behind the peculiar self-regeneration characteristic of the catalytic sites in the DFM.

1. Introduction

Reversing global temperature rise requires mitigating greenhouse gas emissions from the industry and energy sectors (Priorities, 2019). As the world will still rely on fossil fuels in the mid-term, and there are sectors which cannot be easily decarbonised or only partially so, carbon capture and utilization (CCU) technologies are required for the ambitious net zero carbon emission target to be met (Priorities, 2019; Saeidi et al., 2021; Shao et al., 2022; Sun et al., 2023). Recently, the integration of CO_2 capture and its direct conversion into valuable fuels or intermediates such as methane, CO or syn-gas is emerging as a vibrant field of research due to the potential to achieve a circular carbon economy while cutting the costs and increasing the efficiency of the energy-intensive multistep CCU technologies that are currently available (Shao et al., 2022; Sun et al., 2023; Sun et al., 2021; Sun et al., 2021; Merkouri et al., 2021).

In particular, many authors have recently demonstrated that the integrated CO_2 capture and in-situ methanation (ICCM) can be performed over Dual Function Materials (DFMs) (Shao et al., 2022; Sun et al., 2021; Merkouri et al., 2021; Melo Bravo and Debecker, 2019; Omodolor et al., 2020; Kosaka et al., 2021; Chen et al., 2022; Duyar et al., 2016; Kosaka et al., 2022; Duyar et al., 2015; Abdallah and Farrauto, 2022; Bermejo-López et al., 2019; Cimino et al., 2020), which combine at the nanoscale a CO_2 sorbent phase (e.g. alkali (hydro)oxides/carbonates) with a methanation active phase (e.g. Ni or Ru). The process is then operated in a chemical looping mode mediated by the DFM which is alternatively exposed to a CO_2-rich atmosphere (capture stage), and an H_2 stream (methanation stage). Since both CO_2 adsorption and methanation are exothermic the ICCM process can be run isothermally in the 250–350 °C range by harvesting the sensible heat of typical flue gases and without any further energy input (Kosaka et al., 2021; Chen et al., 2022; Duyar et al., 2016), utilizing either fixed bed reactors with alternate feeds (Shao et al., 2022; Melo Bravo and Debecker, 2019; Kosaka et al., 2021; Chen et al., 2022; Duyar et al., 2016) or interconnected fluidized bed reactors with circulating DFM (Kosaka et al., 2022).

As with any chemical looping process, the DFM plays a crucial role and, since the initial works by prof. Farrauto's group (Duyar et al., 2016; Duyar et al., 2015), great efforts have been devoted to the development of advanced formulations which can guarantee significant CO_2 uptake capacity, high catalytic activity and product selectivity, as well as long-term cyclic stability (Sun et al., 2021; Chen et al., 2022; Abdallah and Farrauto, 2022; Bermejo-López et al., 2019; Cimino et al., 2020; Porta et al., 2021; Arellano-Treviño et al., 2019; Jeong-Potter et al., 2022). This is not a trivial matter since, for example, the addition of a sorbent phase (most commonly an alkali (hydro)oxide/carbonate such as Na_2O, K_2O, MgO, CaO, BaO) (Sun et al., 2021; Chen et al., 2022; Porta et al., 2021) to a methanation catalyst (such as Ru/Al_2O_3) can adversely affect the intrinsic activity of the precious metal both in terms of reaction rate and CH_4 selectivity (Cimino et al., 2020; Porta et al., 2021).

* Corresponding author.
E-mail address: stefano.cimino@cnr.it (S. Cimino).

https://doi.org/10.1016/j.ccst.2022.100096
Received 5 December 2022; Received in revised form 22 December 2022; Accepted 24 December 2022

Moreover, when capturing CO_2 from either flue gas or air, the DFM has to be exposed to O_2 and H_2O, which cause pronounced effects on the oxidation state of the catalyst and challenge the stability of performance over multiple cycles (Abdallah and Farrauto, 2022). In particular, Ni-based DFMs can be unsuited to operate in the presence of oxygen, due to the difficult or incomplete reduction of the active phase during the hydrogenation step at T< 300 °C where either CO_2 capture and methanation are thermodynamically favoured (Abdallah and Farrauto, 2022; Arellano-Treviño et al., 2019). By contrast, Ru-based DFMs, despite their higher cost, are easily reduced back to the metal form already at low temperature (above 150 °C) making them the preferred choice (Sun et al., 2021; Merkouri et al., 2021; Chen et al., 2022; Abdallah and Farrauto, 2022). Therefore, state-of-the-art formulations for ICCM with oxidizing flue gases contain Ru (0.5–5% wt) co-dispersed with Na (hydro)oxide onto alumina (Abdallah and Farrauto, 2022). However, ageing in the presence of O_2 and H_2O has been reported to induce extensive sintering of Ru nanoparticles with a consequent permanent deactivation of the DFMs (Jeong-Potter et al., 2022; Bermejo-López et al., 2022).

We have recently reported that lithium doping, differently from other alkali metals, can promote both the CO_2 capture capacity as well as the methanation activity of Ru/Al_2O_3 catalysts (Cimino et al., 2020). As a consequence, $Li\text{-}Ru/Al_2O_3$ DFMs outperform Na-Ru formulations during the ICCM process under ideal conditions (CO_2 in dry N_2) both in terms of methane production and selectivity since they can be optimally operated at lower temperatures (260–280 °C), which could be advantageous for stability issues (Cimino et al., 2022). However, prolonged testing of Li-Ru DFMs is required to extend previous results under more realistic conditions. In particular, apart from O_2 and H_2O, real flue gases often contain contaminants even after purification units, such as NO_x and SO_x (Merkouri et al., 2021), which can potentially affect the performance of DFMs. Those impurities can compete with CO_2 for adsorption sites (Porta et al., 2021; Bermejo-López et al., 2023) and, even worst, low concentrations of sulfur species (≤1ppm) can severely poison catalytic metal sites for hydrogenation (Argyle and Bartholomew, 2015; Kuzmenko et al., 2019; Cimino et al., 2009). As such, sulfur poisoning is a main issue to be addressed when designing and operating CO_2 capture as well as methanation plants, which must be equipped with appropriate gas cleaning units (Merkouri et al., 2021; Kuzmenko et al., 2019; Rönsch et al., 2015).

We have recently shown for the first time (Cimino et al., 2022) that a $Na\text{-}Ru/Al_2O_3$ DFM displays a remarkable and somehow unexpected tolerance to S-poisoning during the ICCM at 300 °C due to a peculiar self-regeneration mechanism of the catalytic sites related to the redo-ox cycle of Ru (Kuzmenko et al., 2019; Cimino et al., 2022). In this work we set out to investigate the performance of a DFM containing Li (3% wt.) and Ru (1% wt.) dispersed on alumina spheres during the integrated CO_2 capture and methanation, assessing the individual and mutual effects of the main species (O_2 and H_2O) found in real flue gas as well as the impact of SO_2 impurities (up to 100ppm). Ru and Li loadings in the DFM were deliberately kept low given the economic concerns for the use of critical raw materials. This helped to highlight the possible deactivation effects during a prolonged ageing study involving more than 100 capture and methanation cycles in a fixed bed reactor operated in the temperature range 260–320 °C with alternate feed conditions. A detailed characterization of fresh and S-aged Li-Ru DFM samples helped to get insights into the mechanism behind the tolerance to sulfur poisoning and long-term stability.

2. Experimental

2.1. Preparation of $Li\text{-}Ru/Al_2O_3$ dual function material

$\gamma\text{-}Al_2O_3$ spheres (Sasol, 1mm nominal diameter, Fig. 1a) were preliminarily washed in a dilute HNO_3 water solution, rinsed with distilled water and finally calcined in air at 450 °C to remove residual basic compounds from their surface. Ru was dispersed onto this support by two consecutive incipient wetness impregnation cycles with a 0.167 M solution of Ru(III) nitrosyl nitrate (Aldrich), each followed by calcination in air at 350 °C for 1h, and final reduction in H_2 (20% in N_2) at 450 °C for 2h (reference sample: RuA). Thereafter, the sorbent phase was added to the RuA catalyst by incipient impregnation with an aqueous solution of $LiNO_3$ (2 cycles), followed by drying at 120 °C in air and reduction in H_2 (20% in N_2) at 450 °C for 2h. The nominal loadings of Li and Ru in the resulting DFM were 3% and 0.95% wt., respectively. Two reference samples were prepared by impregnating the same $\gamma\text{-}Al_2O_3$ spheres with water solutions of $LiNO_3$ or Li_2SO_4, followed by drying at 120 °C.

The freshly reduced DFM was labelled as Li-RuA; the sulfated DFM unloaded from the reactor at the end of the durability study in the presence of SO_2 was named S-Li-RuA. The real density of DFMs was calculated (after stabilization in ambient air for more than 24 h) by weighing a known number of spheres (80–100) having a nominally identical volume (0.523 mm^3).

2.2. Characterization of the DFMs

N_2 adsorption-desorption measurements at 77 K were performed in a Quantachrome Autosorb 1-C after degassing the DFM samples at 150 °C for 3h under a high dynamic vacuum. The specific surface area and pore size distribution (PSD) of the DFMs were evaluated by the BET method and the Non-Linear Density Function Theory (NLDFT, cylindrical pore, equilibrium model), respectively.

The crystal phases of the materials at different stages (fresh, sulfurized) were determined by powder X-ray diffraction (XRD) measurement, using a Rigaku Miniflex 600 diffractometer with Cu Kα radiation (0.154 nm wavelength). XRD patterns were collected in a 2θ range of 10–80 °, with a step of 0.01 ° and 10 °/min counting time. Background correction, fitting, and peak attribution were performed using SmartLab Studio II software. The average crystallite sizes of Ru and $(Li)Al_2O_3$ phases were estimated based on Scherrer's equation from the full width at half maximum (FWHM) of their corresponding main reflections occurring at $2\theta = 43.9°$ [1 0 1] and $2\theta = 66.9°$ [4 4 0], respectively.

FT-IR analysis was performed on self-supported disks of KBr mixed with 2% wt. of powdered DFMs (stabilized in air at room temperature) using a Perkin Elmer Spectrum GX spectrometer with a DTGS detector, with a spectral resolution of 4 cm^{-1}. Each spectrum was averaged over 64 scans and ratioed against the common background spectrum relevant to pure KBr.

A Setaram Labsys Evo TGA-DTA-DSC 1600 flow microbalance was used to perform temperature-programmed reaction tests with DFM samples (90- 100 mg) under a flow of 4.5% H_2/Ar (50 cm^3 min^{-1}) up to 750 °C at a rate of 10 °C min^{-1}. The evolved gases were continuously analyzed by a Mass Spectrometer (Pfeiffer Thermostar G) equipped with a Secondary Electron Detector (MS-SEM), recording the temporal profiles at m/z=2 (H_2), 15 (CH_4), 18 (H_2O), 28 (CO), 30 (NO), 34 (H_2S), 44 (CO_2), (46) NO_2, 64 (SO_2).

2.3. Cycled CO_2 capture and methanation tests in the fixed bed reactor

Combined CO_2 capture and methanation tests were performed in the same fixed bed quartz reactor already described in (Cimino et al., 2022) that was loaded with ca 2.3 cm^3 (packed volume) of Li-RuA. The reactor was operated at atmospheric pressure and at a fixed temperature in the range from 260 °C to 320 °C by switching alternatively the feed between the CO_2 capture and methanation phases while keeping constant the inlet flow rate (20 Sl/h). First, a feed gas stream consisting of 5% vol. CO_2 in N_2 with the possible additional presence of 0.25% O_2 and/or 1.5% H_2O as well as 10–100 ppmv SO_2 was stepwise admitted to the reactor and flowed over the DFM for 18 min (unless otherwise stated). Then, after an intermediate purge step (2 min, under pure N_2), the methanation phase was started by switching the feed to 15% vol. H_2 in N_2 for a total of 14 min (unless otherwise stated). Eventually, the reactor was purged again with N_2, before a new cycle was started. In some experiments,

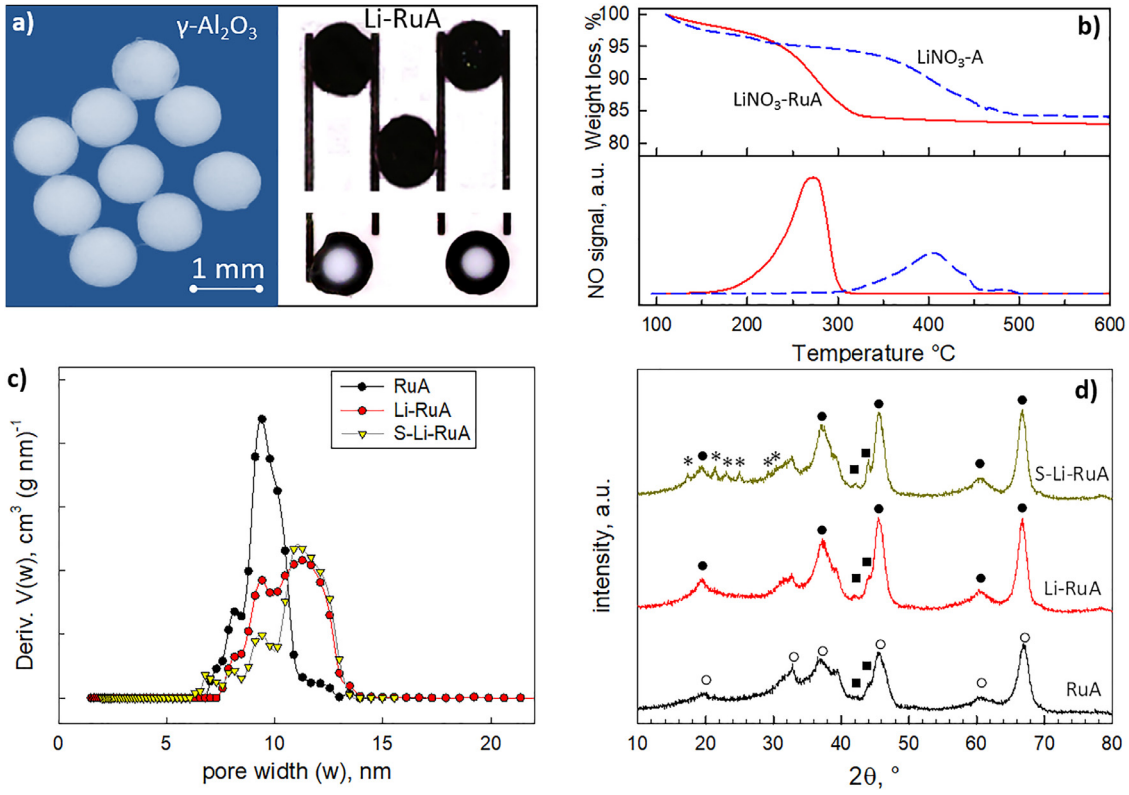

Fig. 1. (a) Optical images of spherical γ-Al_2O_3 support and blade cut cross-sections of Li-RuA DFMs prepared with or without preliminary washing the support in acidic solution determining a homogeneous or an egg-shell distribution of Ru (black) within the spheres. (b) Weight change and corresponding emission trace of NO during the H_2-reduction of $LiNO_3$ impregnated on either RuA catalyst and bare Al_2O_3 support. (c) Pore Size Distribution analysis and (d) XRD patterns of the fresh reduced RuA and Li-RuA DFM and its aged form (S-Li-RuA) as recovered at the end of the prolonged tests of cyclic CO_2 capture with SO_2 and methanation. XRD Legend: ■ =Ru, o =γ-Al_2O_3, * =Li_2SO_4, ● = $LiAl_5O_8$

the CO_2 capture step was performed as previously described (at a fixed temperature in the range 180–280 °C), whereas the methanation phase was run under a temperature-programmed mode by heating the reactor to 300 °C at 10 °C min^{-1} (keeping constant the total duration of 14 min under H_2 flow).

The molar fractions of CO_2, CH_4, CO, and SO_2, H_2S were measured by two continuous gas analyzers (ABB Optima Advance) equipped with ND-IR and UV detectors, respectively. Therefore, the quantities of CO_2 and SO_2 captured or desorbed by the DFM, as well as those of CH_4, CO and H_2S formed, were calculated by integrating their corresponding temporal concentration traces after correction for the gas hold-up in the empty reactor. The overall carbon balance was generally closed within ±2%. The CO_2 conversion was calculated based on the total carbon-species released during the catalytic hydrogenation stage.

2.4. Catalytic CO_2 methanation tests

Catalytic methanation tests of gaseous CO_2 were run as described in (Cimino et al., 2020; Cimino et al., 2022) using the same fixed bed quartz reactor that was loaded with ca 0.62 cm^3 (packed-volume) of DFM spheres. Before testing, DFM samples were pre-reduced in-situ at 400 °C under 20% vol. H_2/N_2, except for the S-Li-RuA sample recovered to ambient air after the prolonged ageing study. Temperature-programmed reaction tests were performed at ca 3 °C min^{-1} from 200 °C under a flow of $CO_2/H_2/N_2$ = 1/4/5 that was fed to the reactor at a Gas Hourly Space Velocity (GHSV) = 32500 h^{-1}. The conversion of CO_2 and the selectivity to CH_4 were continuously calculated from the molar fractions of CO, CO_2, and CH_4 in the product stream. The rate of CO_2 consumption per unit mass of Ru in the DFM ($R_{Ru}CO_2$) was estimated from low conversion data (<10%) assuming isothermal behaviour, differential conditions, and constant molar flow rate. The Arrhenius plot of $R_{Ru}CO_2$ was used to estimate the apparent activation energy for the catalytic CO_2 hydrogenation.

3. Results and discussion

3.1. Characterization of fresh Li-RuA DFM

It is well known that the dispersion of Ru on alumina pellets or spheres by impregnation with aqueous solutions often leads to an egg-shell distribution due to a limited penetration depth of the noble metal (Cimino et al., 2020; Porta et al., 2020) attributed to the strong interaction with the surface and the precipitation of Ru-hydroxide species even under acidic conditions (Povar and Spinu, 2016). However, by preliminary washing the γ-Al_2O_3 spheres with a diluted nitric acid solution it was possible to obtain a homogeneous distribution of Ru throughout the particles, confirmed by the uniform dark colouration of blade-cut cross sections of the Li-RuA particles (Fig. 1a, top right). This contrasts with the egg-shell distribution of Ru previously found in similar Li-RuA materials (Fig. 1a, bottom right), which were prepared using identical precursors and methods but without any pretreatment of the commercial γ-Al_2O_3 support (Cimino et al., 2022).

Dispersion of the CO_2-sorbent phase onto RuA spheres was performed by impregnation with $LiNO_3$ precursor solution and the subsequent reduction step was analyzed by TG-MS (Fig. 1b). The presence of the active Ru metal significantly lowered the decomposition temperature of $LiNO_3$ which started already from 175 °C (i.e. below its melting point at 255 °C) and was completed at ca 300 °C, as testified by the corresponding NO emission trace. For comparison purposes, the decomposition of $LiNO_3$ when dispersed on bare γ-Al_2O_3 spheres

Table 1
Summary of the characterization results for (reduced) Ru/A, Li-Ru/A, and S-Li-Ru/A DFM: Density of the spheres, Specific surface area (S_{BET}), mesopore volume (V_{mesoP}), and pore width by N_2 physisorption; dimensions of Ru (d_{Ru}) and Al_2O_3 (d_{Al2O3}) crystallites from XRD data; S content; apparent activation energy values (E_a) and temperatures for 10% conversion (T_{10}) for the catalytic hydrogenation of gaseous CO_2.

	Density g cm^{-3}	S_{BET} m^2 g^{-1}	V_{mesoP} cm^3 g^{-1}	Pore width (mode) nm	d_{Ru} nm	d_{Al2O3} nm	S content % wt.	E_a kJ/mol	T_{10} °C
RuA	1.40	180	0.44	9.4	10.3	5.5	-	71	293
Li-Ru/A	1.53	145	0.40	10.9	10.6	6.4	-	81	265
S-Li-Ru/A	1.59	133	0.36	11.3	16.5	6.6	2.1[a]	71	303[b]

[a] estimated from the TG-MS analysis supposing the decomposition of Li_2SO_4 into Li_2O.
[b] S-aged DFM sample recovered to air and tested without any further pretreatment.

started above 300 °C and required ca 500 °C to be completed (Fig. 1b). It follows that Li-nitrates possibly formed during the CO_2 capture stage from flue gases containing some NO_x would be catalytically decomposed during methanation at ca 300 °C, in good agreement with recent results over Ru-Ba/Al_2O_3 and Ru-Na-Ca/Al_2O_3 DFMs (Porta et al., 2021; Bermejo-López et al., 2023): therefore, NO_x impurities are not expected to severely impact ICCM process performances.

Textural and morphological properties of the fresh Li-RuA material as well as its parent RuA catalyst are presented in Table 1.

The dispersion of Li on RuA induced a 9.2% increase in the density of the resulting DFM spheres (stabilized in air after reduction). However, the specific surface area of Li-RuA was lowered by as much as 19% with respect to RuA (from 180 down to 145 m^2 g^{-1}), suggesting a deeper modification of the original textural properties of the parent material. In particular, the Pore Size Distribution analysis (Fig. 1c) indicates Li-addition caused an evident enlargement of the average dimension of the mesopores (Table 1) that passed from 9.4 nm for RuA (and its bare support) up to 10.9 nm for Li-RuA. At variance, Na addition (3% wt.) to a similar RuA material, did not alter the initial textural features (Cimino et al., 2022). Accordingly, a direct comparison of the XRD patterns relevant to freshly reduced Li-RuA and RuA samples (Fig. 1d) indicates Li addition induced a small shift and an increase in the intensity of all the main peaks characteristic of the γ-Al_2O_3 support (2θ ca 19.4 °, 37.3 °, 45.5 °, 66.9 °). This was already assigned to the formation of the mixed $LiAl_5O_8$ crystalline phase (PDF# 3-911) (Cimino et al., 2022), which shares the same spinel structure of γ-alumina with almost identical lattice parameters (Narayanan and Uma, 1987). Interestingly, the estimated average size of the Al_2O_3 crystallites increased by ca 20% due to the formation of the Li-aluminate phase (Table 1), thus justifying the corresponding enlargement of the pore size. Moreover, upon prolonged exposure to ambient air two additional signals at 2θ 11.7 ° and 23.5 ° appeared in the XRD pattern of Li-RuA (not shown) that can be assigned to the spontaneous formation of the hydrotalcite-like $Li_2Al_4(CO_3)(OH)_{12}$-$3H_2O$ (PDF# 37–728), which reversibly decomposes above 250 °C under inert flow (Cimino et al., 2022). The peaks at 2θ ca 42.0 ° and 43.9 ° correspond to the main reflections of metallic Ru. The characteristic dimensions of the metal crystallites (d_{Ru}) in RuA and Li-RuA, estimated by Scherrer's equation, were equal to 10.3±0.7 and 10.6±0.8 nm, respectively (Table 1): therefore, Li addition and the subsequent reduction of the DFM at 450 °C did not alter the initial metal dispersion.

The 10 nm size of the Ru nanoparticles was largely dictated by the oxidative treatment in air at 350 °C after impregnation (Chin et al., 2005), which, however, is required to stabilize the DFM for operation under alternate oxidizing/reducing feed conditions. Indeed, it has been recently reported (Jeong-Potter et al., 2022) that a 1% Ru, 6% "Na_2O"/Al_2O_3 DFM with high initial metal dispersion (d_{Ru} ca 2–3 nm), which was not pre-oxidized/stabilized, suffered severe metal sintering (final d_{Ru} ca 36–37 nm) during repeated cycles of CO_2 capture from simulated power plant effluent (with 4.5% O_2) and methanation at 320 °C. Ru sintering was identified as the main cause of permanent loss of methanation activity (Jeong-Potter et al., 2022).

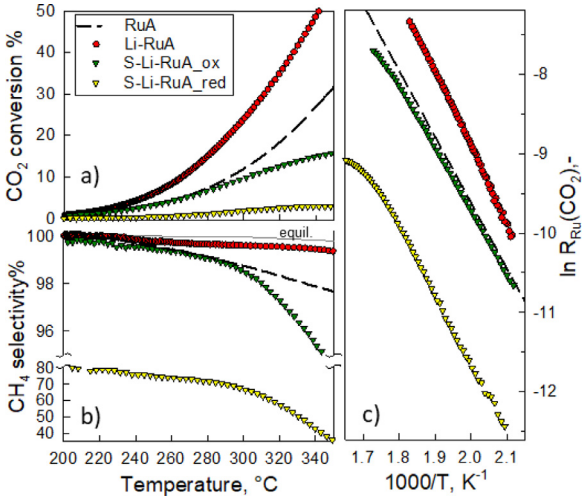

Fig. 2. CO_2 conversion (a), selectivity to CH_4 (b) as a function of the reaction temperature and corresponding Arrhenius plots for the CO_2 consumption rate during the catalytic methanation tests over fresh RuA, Li-RuA, and sulfated S-Li-RuA samples (either oxidized and reduced form). Feed composition: $CO_2/H_2/N_2$ = 1/4/5, GHSV = 32500 h^{-1}. The solid line in panel b corresponds to the thermodynamic equilibrium curve. Experimental details can be found in Section 2.7.

It is worth noting that the homogeneous distribution of Ru nanoparticles inside the alumina spheres (achieved via the acidic-wash pretreatment of the support) enhanced the metal dispersion if compared to our previous results on analogue Ru-based DFMs (Cimino et al., 2022) having an egg-shell distribution of the metal (d_{Ru} ca 16 nm).

Temperature-programmed methanation tests were performed co-feeding CO_2 and H_2 over Li-RuA and its parent RuA catalyst to confirm the peculiar promoting effect of Li, at variance to other alkali metals such as Na and K (Cimino et al., 2020; Porta et al., 2021): results are presented in Fig. 2 in the form of CO_2 conversion and CH_4 selectivity plots as well as Arrhenius plots for the catalytic CO_2 consumption rate. Li-addition to RuA significantly promoted the methanation activity in the whole temperature range (Fig. 2a) so that the temperature for 10% conversion decreased from 293 °C down to 265 °C (T_{10}, Table 1), and the process selectivity to CH_4 more closely approached the thermodynamic equilibrium curve (Fig. 2b). Specifically, the catalytic reaction rate per unit mass of Ru more than doubled (x2.4) at 265 °C. At the same time, the apparent activation energy of the reaction raised from ca 71 kJ mol^{-1} up to 81 kJ mol^{-1}, in very good agreement with previous results (Cimino et al., 2022). Interestingly, the RuA catalyst with a uniform metal distribution prepared in this work was twice as active as its counterpart with an egg-shell distribution (Fig. S1, Supplementary Material): this correlates well with the increased number of Ru active sites which are conveniently located at the nexus of the metal, support, and

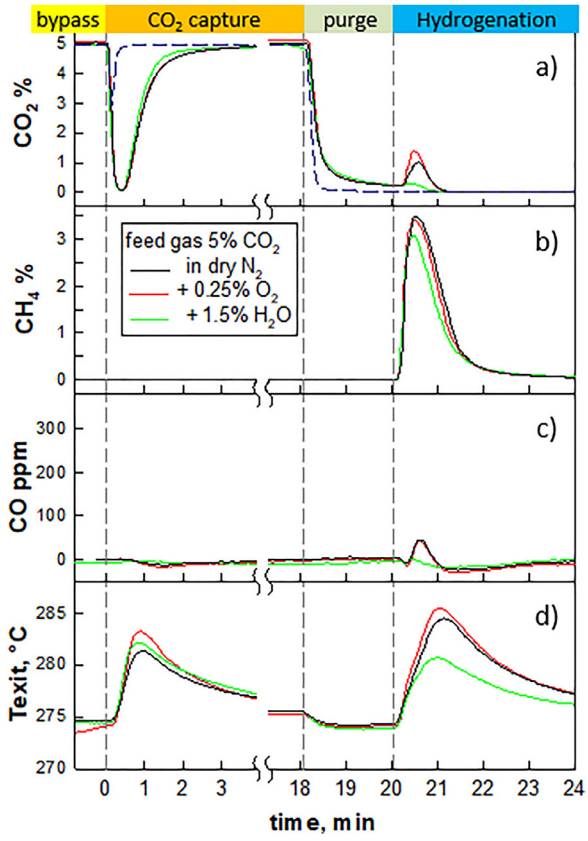

Fig. 3. Integrated CO_2 capture and methanation cycles on Li-Ru/A DFM operating at 280 °C with 3 different feed gas compositions during adsorption: 5% CO_2 in N_2 (black lines), with the addition of +0.25% O_2 (red lines) or +1.5% H_2O (green lines). Temporal outlet concentrations of CO_2 (a) CH_4 (b) and CO (c), and temperature profiles as measured at the exit of the catalytic bed (d). Step duration: 18 min CO_2 capture, 2 min N_2 purge, 14 min hydrogenation (15% H_2 in N_2). Dashed line in (a) represents the reactor hold-up.

atmosphere i.e. along the perimeter of the supported metal nanoparticles, whose length scales as $(d_{Ru})^{-2}$ at fixed loading (Cargnello et al., 2013).

3.2. Integrated CO_2 capture and methanation in the fixed bed reactor

3.2.1. Effect of flue gas composition and reaction temperature

A single batch of Li-Ru/A DFM was used to perform a parametric study of the integrated CO_2 capture and methanation process aiming to elucidate the individual effects of O_2 and H_2O when added to a feed gas containing 5% CO_2 in N_2. Fig. 3 presents the typical transient CO_2, CH_4, and CO concentration traces as well as the temperature profiles recorded at the exit of the DFM bed during standard cycles run at a fixed preheating (280 °C). As soon as admitted to the reactor, CO_2 was quickly captured by the DFM (Fig. 3a) so that its concentration dropped to zero after ca 25 s independently from the presence of O_2 or H_2O in the feed stream; thereafter, it started to raise progressively until the overall capacity was mostly saturated (within 4 min). The contribution from the reactor hold-up can be visualized by the dashed line in Fig. 3a. Some weakly bonded CO_2 was spontaneously desorbed from the DFM during the intermediate purge phase under N_2 flow (required to avoid gas mixing) before H_2 was admitted to the reactor to start the hydrogenation phase. At that point, CH_4 formation occurred with an apparent initial rate that was not affected by the eventual presence of O_2 or H_2O during the previous stage. The peak production of CH_4 (up to 3.5% by volume) was achieved within 25s, being slightly lower when the simulated feed gas contained some H_2O, due to the lower amount of CO_2 stored on the

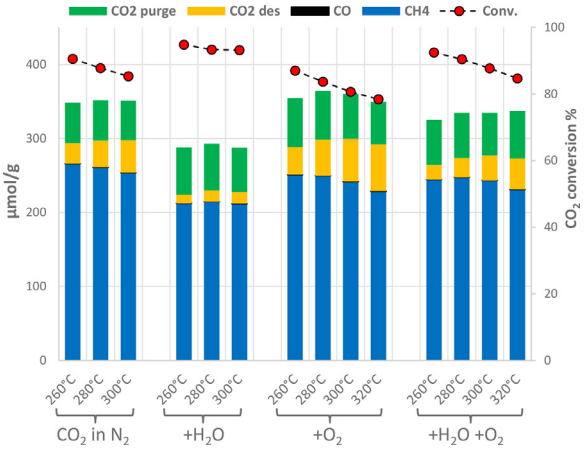

Fig. 4. Effect of the feed gas composition and the reaction temperature on the average values of CH_4 and CO produced, CO_2 desorbed and purged (bars), CO_2 conversion (dots) during 3 consecutive cycles of integrated isothermal CO_2 capture and methanation with Li-RuA DFM. Adsorption conditions: 5% CO_2 in N_2 (reference case) with the eventual addition of 1.5% H_2O, 0.25% O_2, or both. Experimental details can be found in Section 2.6.

DFM. Simultaneously, a very low amount of CO was formed (≤40ppm, Fig. 3c), and it became almost undetectable for the humid flue gas case. A limited thermal desorption of CO_2 was observed at the beginning of the hydrogenation phase (Fig. 3a), driven by the heat released by the exotherm of the catalytic reaction, which indeed caused a temperature increase recorded at the exit of the DFM bed (Fig. 3d). The maximum and minimum values of ΔT_{exit} were measured when the flue gas contained O_2 or H_2O, respectively.

Interestingly, also the CO_2 capture process caused similar temperature increases due to the exothermic nature of the surface reactions involved, which increased in the presence of O_2 in the flue gas (Fig. 3d). In particular, at temperatures exceeding 200 °C Ru can be easily oxidized during adsorption and then reduced back to its metal form during the methanation step: both the oxidation of Ru by O_2 and the reduction of RuO_x by H_2 are exothermic reactions (Porta et al., 2021) which therefore contribute to enhancing the heat release during each half cycle (Fig. 3d). It can be argued that the Ru content in the DFM (as well as any other reducible metal oxide such as NiO_x or CeO_x) should be kept as low as possible to limit the extent of the parasitic H_2 consumption to form water (Abdallah and Farrauto, 2022).

The parametric study was further extended to investigate the effect of the average reaction temperature in the 260–320 °C range. A minimum of three adsorption-reaction cycles were run for each specific test condition giving highly repeatable results: the average values are summarized in Fig. 4 reporting the CH_4, CO and CO_2 released during the methanation, the resulting CO_2 conversion, and the CO_2 lost during the intermediate purge. All relevant data, including the C-balance, selectivity to CH_4 and maximum temperature gradients recorded during adsorption and reaction half-cycles are also listed in Table S1.

The Li-RuA DFM displayed a cyclic CO_2 capture capacity of ca 350 μmol/g under reference conditions (CO_2 in dry N_2) that was poorly affected by the operating temperature in the range explored herein. The presence of water vapour in the feed gas reduced it by ca 16–19% with respect to dry conditions, whereas the addition of O_2 showed a marginally positive effect (ca 2–4%). The amount of CO_2 released during the purge phase was almost constant, but the CO_2 desorbed during the methanation increased at higher temperatures as well as in the presence of O_2, and decreased under humid conditions. Accordingly, the CO_2 conversion during methanation showed a decreasing trend with temperature passing from 90.6% at 260 °C to 85.3% at 300 °C under reference conditions (Fig. 4). Moreover, it was higher with humid rather than with O_2-containing feed (Table S1). CO production was always very

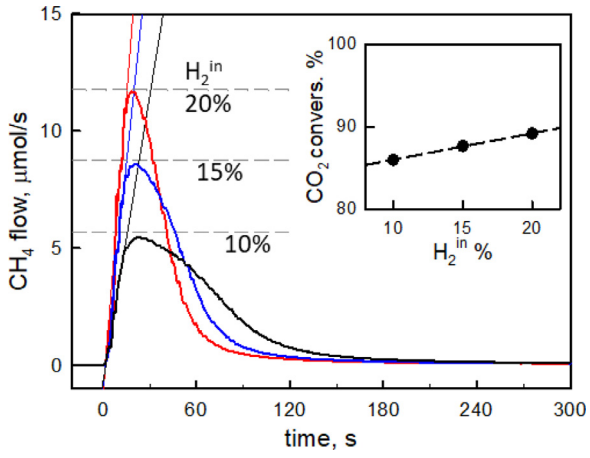

Fig. 5. Methane production rates from CO_2 preadsorbed over Li-RuA DFM as a function of the inlet partial pressure of H_2 at 300 °C. Adsorption conditions: 5% CO_2, 1.5% H_2O, 0.25% O_2 in N_2 for 9 min. Dashed horizontal lines correspond to the maximum theoretical CH_4 flow depending on the H_2 feed rate. Inset: CO_2 conversion at the end of the methanation phase (7 min).

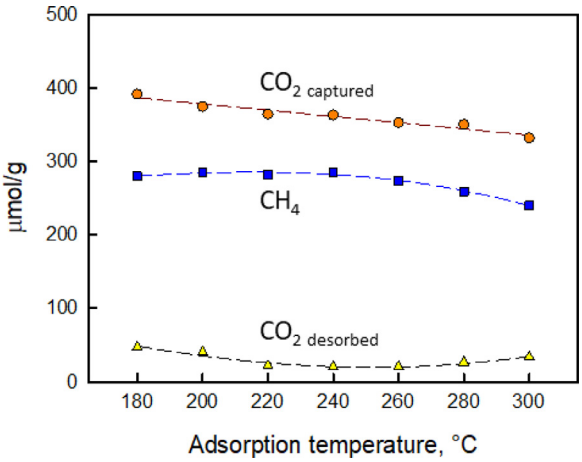

Fig. 6. Effect of the adsorption temperature on the CO_2 capture as well as the CH_4 and CO_2 released during the subsequent temperature programmed methanation (10 °C min^{-1} up to 300 °C, then hold) with Li-RuA DFM. Adsorption conditions (18 min): 5% CO_2, 1.5% H_2O, 0.25% O_2 in N_2. Experimental details can be found in Section 2.6.

small but it became negligible under humid conditions and for temperatures up to 300 °C (Table S1). Water retained on the surface of the DFM during adsorption can inhibit the formation of CO upon the injection of H_2 by shifting the water gas shift equilibrium reaction ($H_2 + CO_2 \leftrightarrow CO + H_2O$).

Eventually, when O_2 and H_2O were simultaneously present in the simulated flue gas, their individual thermal and chemical effects partially compensated, so that, for example, the associated penalty in the CO_2 capture capacity was favourably limited to only ca 5% with respect to the reference case. This resulted in a maximum methane production of 247±3 $\mu mol/g_{DFM}$ achieved at as low as 280 °C, with an outstanding 99.98±0.01% selectivity and a CO_2 conversion exceeding 90%; similar performances were also achieved at 260 °C (Table S1). While further improvements of the specific methane production are possible by increasing the Li loading in the DFM (at least up to 5% wt, (Cimino et al., 2022)), this was deliberately kept low to better highlight durability and poisoning issues during reaction ageing with SO_2-loaded flue gas (see Section 3.2.4). For comparison purposes, a similar Na-RuA DFM (same metal and alkali loadings) tested by us under identical rector configuration and experimental conditions returned a maximum CH_4 production equal to 183±2 $\mu mol/g_{DFM}$ (@300 °C) with 99.73±0.03% selectivity and 89% CO_2 conversion (Cimino et al., 2022). Notably, the favourable and unique synergy existing between Li and Ru phases in the DFM guarantees a 20–60 °C reduction for the optimal operating temperature of the integrated process with respect to state-of-the-art Na-Ru DFMs (Merkouri et al., 2021): this is particularly important in view of the long term durability of the DFM (Jeong-Potter et al., 2022; Bermejo-López et al., 2022).

3.2.2. *Effect of H_2 concentration during methanation*

A further set of experiments at 300 °C were run to investigate the effect of the H_2 concentration during the methanation phase following a CO_2 capture stage (9 mins) from a humid feed gas also containing O_2. As shown in Fig. 5, at increasing the H_2 concentration from 10 to 15 and 20% the methane production became faster and the methane peak sharper. In particular, the slopes of the initial methanation rate profiles scaled proportionally to the concentration of hydrogen (0.41, 0.63 and 0.84 mmol s^{-2}). In each case, the peak production rate reached after ca 20 s corresponded to the complete consumption of all the H_2 fed to the reactor. It can be argued that the methanation of the CO_2 preadsorbed on the Li-RuA DFM initially proceeded with an apparent first-order dependence on the partial pressure of H_2 and probably under mass transfer control. The fast initial methanation rate can be explained by the fast reaction of highly reactive CO_2 ad-species/carbonates stored onto the Li-Al sites, which can easily spill-over onto vicinal Ru sites that are reduced back to the metal form as soon as exposed to H_2 (Arellano-Treviño et al., 2019; Cimino et al., 2022).

After the methane peak, the formation rate became limited by the availability of residual CO_2 on the DFM, thus showing a faster drop for larger concentrations of H_2. The faster methanation rate achieved at higher H_2 concentration promoted the overall CO_2 conversion (inset in Fig. 5) since less CO_2 was thermally desorbed from the DFM and lost before it could react with the incoming H_2 flow.

3.2.3. *Effect of the CO_2 adsorption temperature*

It was previously recalled that the CO_2 adsorption on pre-reduced alkali-based DFMs is an exothermic process that is thermodynamically favoured at lower temperatures where it can still occur with fast kinetics (Jeong-Potter et al., 2022). At variance, the catalytic methanation of CO_2 over Ru-alumina catalysts proceeds at a low rate below 200 °C but is more strongly activated by the temperature (Fig. 2).

To investigate the potential of operating the two half-cycles at different temperatures we lowered the temperature during the isothermal CO_2 capture stage (down to 180 °C in 20 °C intervals) while the subsequent hydrogenation was performed in a temperature-programmed mode by heating the reactor at ca 10 °C/min up to 300 °C (keeping constant the total duration of 14 min). Results presented in Fig. 6 confirm that the CO_2 capture capacity of the Li-RuA DFM almost linearly increased from 330 $\mu mol/g_{DFM}$ at 300 °C up to 390 $\mu mol/g_{DFM}$ at 180 °C. As a consequence, methane production was enhanced with respect to the reference case of isothermal operation at 300 °C (243 $\mu mol/g_{DFM}$) reaching a maximum of 285 $\mu mol/g_{DFM}$ when CO_2 capture was performed at 240 °C. The amount of CO_2 lost during the methanation phase increased progressively when the initial temperature was below 240 °C, due to competition between thermal desorption and (initially slow) surface reaction (Jeong-Potter et al., 2022), which penalizes the CO_2 conversion and limits its methane yield. As such, higher concentrations of hydrogen and larger amounts of DFM can help to speed up and light off the methanation reaction also taking into account the internal heating effect due to the exothermal release.

While fast external heating of a full-scale fixed bed reactor unit in between the capture and hydrogenation steps might be problematic (Jeong-Potter et al., 2022), running the integrated process with two interconnected fluidized bed reactors with circulating DFM particles (Kosaka et al., 2022) could allow to independently optimize the operating temperature of each reactor.

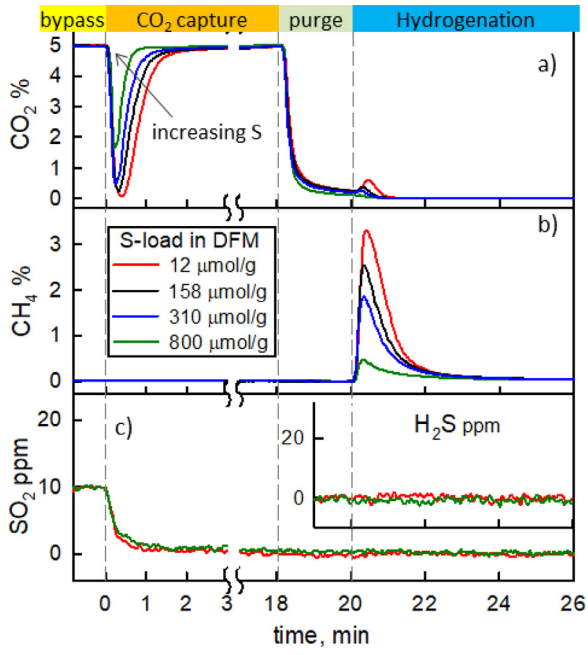

Fig. 7. Integrated CO_2 capture and methanation cycles on Li-RuA DFM operating at 280 °C with a simulated flue gas containing 5% CO_2, 1.5% H_2O, 0.25% O_2 and 10 ppmv SO_2 at different ageing points (reported as S-loads captured on the DFM). Temporal outlet concentrations of (a) CO_2, (b) CH_4, (c) SO_2 and H_2S. Step duration: 18 min CO_2 capture, 2 min N_2 purge, 14 min hydrogenation (15% H_2 in N_2).

Overall, the same batch of Li-RuA DFM performed 81 cycles of integrated CO_2 capture and methanation for the parametric study without any significant sign of degradation of its initial performance.

3.2.4. *Effect of SO_2 and long term ageing*

Eventually, we set out to investigate the performance and stability of the Li-RuA DFM over time when SO_2 (10 or 100 ppm) was co-fed with CO_2 in the simulated flue gas also containing H_2O and O_2. During the capture step, the exit gas concentration of SO_2 quickly dropped to zero while, during methanation, the Li-RuA DFM did not emit any measurable H_2S (nor SO_2) (Fig. 7) but retained all of the sulfur fed to the reactor. This is not surprising given the strong affinity of alkali-based sorbents for SO_2 leading to the formation of stable sulfite/sulfates (Cimino et al., 2022; Das et al., 2001). Therefore, the general performances measured during the ageing study at 280 °C are presented in Fig. 8 in terms of the SO_2 removal efficiency, CO_2 capture, CH_4 (and H_2S) production, CO_2 conversion, and CH_4 selectivity, as a function of the total amount of sulfur stored on the DFM. In particular, empty and close symbols refer to tests performed with either 10 or 100 ppm of SO_2, respectively. For comparison purposes, the black dash-dotted lines in Fig. 8b,c report data relevant to our previous results obtained with a Na-RuA DFM (Cimino et al., 2022).

Initially, the Li-RuA DFM showed remarkable tolerance to the presence of SO_2 in the flue gas as all process outcomes were almost unaltered up to ca 70 $\mu mol/g_{DFM}$ of stored S. Thereafter, the CO_2 capture capacity and the corresponding CH_4 production started to decrease progressively following almost parallel trends, while the CO_2 conversion and CH_4 selectivity remained close to their original values or even increased slightly. This is a clear indication that SO_2 competed with CO_2 for the same basic adsorption sites of the DFM, which, once saturated with S-species, were not restored during the hydrogenation phase. Notably, the intrinsic catalytic methanation activity of Ru sites was substantially preserved even at high S-loadings, as also confirmed by a close inspection of the temporal CH_4 production profiles (Fig. 7b) that showed no initial delay and identical initial formation rates. Furthermore, the performance enhancement measured over the Li-based DFM as compared to its Na-based counterpart (ca 35–40% larger capture capacity and methane production, Fig. 8b, c) was preserved along with the increasing S-load over time on stream.

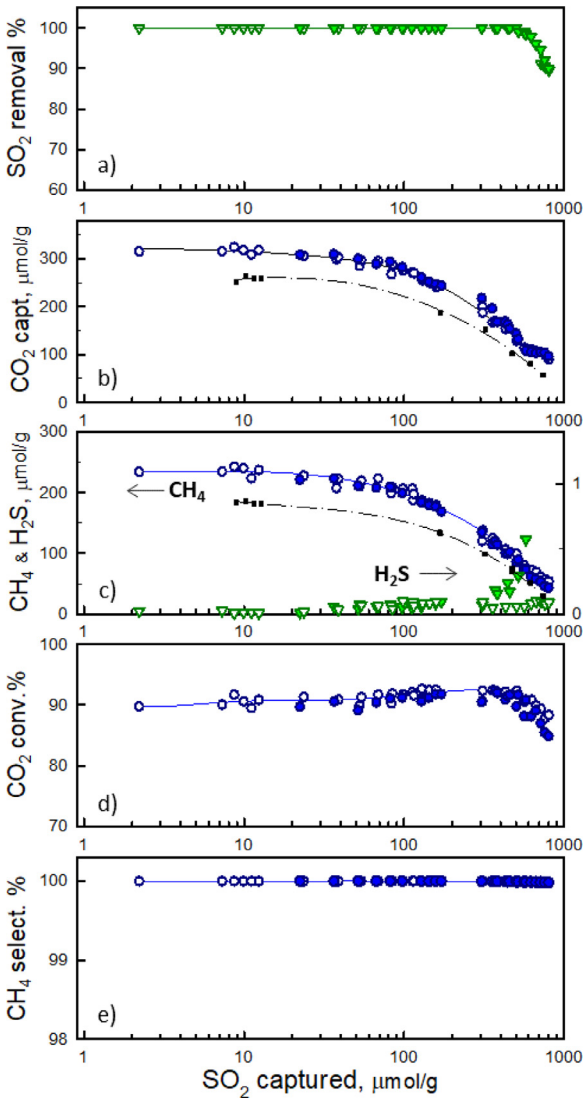

Fig. 8. Integrated CO_2 capture and methanation cycles on Li-RuA DFM operating at 280 °C with a simulated flue gas containing 5% CO_2, 1.5% H_2O, 0.25% O_2, and 10 or 100 ppmv SO_2 (open or closed symbols, respectively). SO_2 removal efficiency (a) and CO_2 capture (b), CH_4 and H_2S production (c), CO_2 conversion (d), and CH_4 selectivity (e) as a function of the cumulative amount of SO_2 retained on the DFM across cycles. Black dash-dot lines correspond to data measured on a Na-RuA DFM (Cimino et al., 2022).

The removal efficiency for SO_2 approached a breakthrough condition (90 %) at ca 800 $\mu mol_{SO2}/g_{DFM}$ corresponding to a S/Li atomic ratio around 0.2: at that point, the residual CO_2 uptake and CH_4 production were reduced to ca 25 % of their original values but the initial high conversion and selectivity values were still preserved and no H_2S was detected (inset in Fig. 7c).

As shown in Figs. 8c and S2, some H_2S started to be formed during the hydrogenation phase once the S-loading on the DFM approached the saturation level and the feed SO_2 concentration was raised to 100 ppm. This result indicates a higher reactivity of "last-captured" sulfur species that were more weakly bonded to the DFM surface. Qualitatively similar results were previously found over a Na-RuA DFM operating at 300 °C, which, however, released some small amounts of H_2S already

before being fully sulfated (Cimino et al., 2022). The higher stability of Li-rather than Na- sulfate species formed on the DFM directly translates into a higher purity of the synthetic natural gas stream which does not require further purification to remove H_2S traces.

While S-species captured on the strong basic sites of the Li-RuA DFM appear too stable to be hydrogenated at 280 °C, it is suggested that more weakly bonded SO_x ad-species on a mostly saturated DFM surface can spill-over onto adjacent catalytic sites to form H_2S (Cimino et al., 2022; Kuzmenko et al., 2019). A close inspection of the transient emission profiles in Fig. S2 reveals that the formation of H_2S was somehow delayed and only started after the peak production of methane was achieved, indicating it required a clean Ru surface (not covered by CO_x species) to proceed.

It should be mentioned that Ru-based catalysts are generally prone to severe poisoning effects by sulfur under reducing atmospheres due to the easy formation of inactive and stable metal sulfide species (Kuzmenko et al., 2019): at variance, we did not observe any evident loss of catalytic activity (as measured by the CO_2 conversion and CH_4 selectivity), even in those last experiments run with a highly sulfated DFM when H_2S was detected in the product stream (Figs. 8 c,d and S2) and RuS_x species were likely formed during the methanation phase.

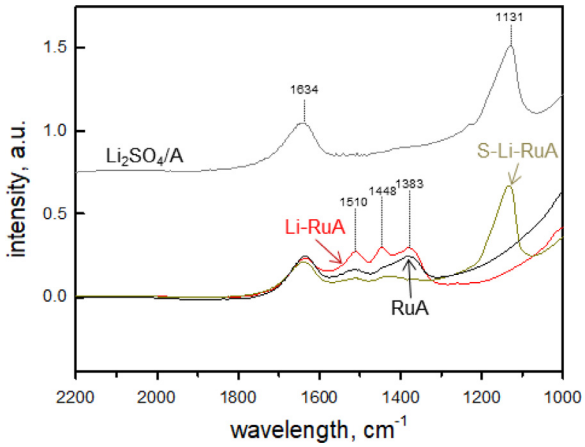

Fig. 9. FT-IR spectra recorded on air-stabilized samples of RuA (black), Li-RuA (red) and S-Li-RuA (dark yellow) recovered at the end of the ageing study. The (grey) spectrum in the upper part of the panel refers to the reference Li_2SO_4/A sample. Experimental details can be found in Section 2.4.

3.2.5. *Characterization of the sulfur-aged DFM*

At the end of the S-aging study, the S-Li-RuA DFM was recovered to air and characterized after having completed a total of 108 CO_2 capture and methanation cycles during 50 days in the reactor (at temperatures in the range 260–300 °C).

The accumulation of sulfur on the DFM caused a slight increase in the density of the spheres (Table 1). Several additional small peaks appeared in the XRD pattern of the S-Li-RuA sample (Fig. 1d), which can all be assigned to the formation of the crystalline Li_2SO_4 phase (PDF 15–873). The average crystallite size of the Li-Al spinel support in the S-aged DFM increased marginally as compared to the fresh sample (up to 6.6 nm). Accordingly, the prolonged ageing induced minor textural modifications in the S-Li-RuA sample, which retained a specific surface area as high as 133 m^2/g (i.e. ca 8% lower than the fresh DFM, Table 1) due to a slight loss of contribution from mesopores with a characteristic size around 9 nm (Fig. 1c). Ru crystallites increased their average size up to ca 16.8 nm (Table 1), suggesting some metal sintering had occurred upon ageing, though this was probably overestimated due to an unresolved contribution coming from the Li-sulfate phase at 2θ angle ca 44 °. Even so, the noble metal in the Li-RuA DFM displayed satisfactory stability against sintering, much better than what observed upon ageing of a 1% Ru, 6.1%"Na_2O"/Al_2O_3 DFM cyclically operating at 320 °C with larger concentrations of steam and oxygen (15% and 4.5%, respectively) (Jeong-Potter et al., 2022).

FT-IR spectra of the aged S-Li-RuA sample and its freshly reduced RuA and Li-RuA counterparts after stabilization in air are compared in Fig. 9. Prolonged cyclic operation in the presence of SO_2 caused the appearance of a strong band peaked at 1131 cm^{-1}, which was previously assigned to sulfate-like species on alumina or alkali-doped alumina (Corro et al., 2002; Waqif et al., 1992). The same band was unambiguously detected in the spectrum of the reference Li_2SO_4/A material (Fig. 9). In the spectral region 1600–1300 cm^{-1}, typical of CO_2 adsorbed on oxide supports (Du et al., 2010), the fresh Li-RuA DFM showed a more complex and intense signal compared to its parent RuA material. In particular, Li addition significantly enhanced all the main signals detected at 1510, 1448, and 1383 cm^{-1}, in line with its promoting effect on both weak as well as medium-strength CO_2 sorption (Cimino et al., 2020; Cimino et al., 2022). Similarly, additional carbonates bands were reported upon potassium doping of alumina (Montanari et al., 2011), which were assigned to the formation of bidentate carbonates partially replacing bicarbonates usually formed on Al- hydroxylated sites. By contrast, no signals were present in the spectral region of the carbonates for the reference sample, indicating that the dispersion of 10% wt. Li_2SO_4 on alumina almost completely hindered CO_2 adsorption. Therefore, the small residual signals detected on the S-Li-RuA DFM at 1510 and 1430 cm^{-1} indicate that not all of the basic Li-Al (or Al) sites on the surface were saturated by sulfate species, which agrees with the residual (25%) CO_2 capacity measured at 280 °C at the end of the ageing study. The unaltered band at 1634 cm^{-1} assigned to the bending vibration of H_2O (Rege and Yang, 2001) indicates that the deposition and/or formation of Li-sulfates did not hinder water adsorption on the materials.

TG-MS analysis of the aged S-Li-RuA sample under H_2 flow (Fig. S3) displayed a characteristic weight loss event (-5.1 %) in the temperature range 460–700 °C (giving a DTG peak at ca 615 °C), which was accompanied by the simultaneous release of SO_2, H_2S and H_2O: this corresponds to the reactive decomposition of Li_2SO_4 when supported on alumina (reference sample in the same figure). For comparison purposes, sodium sulfates, which formed upon S-aging of a Na-RuA DFM, showed lower stability under H_2 and started to decompose around 400 °C (Cimino et al., 2022). The total amount of sulfur stored on the aged S-Li-RuA sample was thus estimated equal to 2.1 % wt. (Table 1), which closely matched the quantity of SO_2 removed from the flue gas during the cyclic operation of the DFM.

Eventually, the intrinsic catalytic activity of the S-Li-RuA DFM was investigated on the aged sample recovered to air (i.e. in oxidized form, without further pretreatment) using the standard temperature programmed protocol from 200 °C under the CO_2+H_2 flow. As shown in Fig. 2, the prolonged S-aging caused some loss of activity: in particular, the CO_2 conversion (rate) and CH_4 selectivity plots relevant to the S-Li-RuA DFM were roughly superimposed to the corresponding plots recorded over the fresh, unpromoted RuA sample up to ca 280–290 °C. Above this threshold temperature, the selectivity to CH_4 dropped faster for the S-Li-RuA sample, and the overall reaction rate only increased marginally along with the increasing temperature (Fig. 2c). It can be argued that in the low temperature region (up to 280 °C), the unavailability of free Al-Li sites close to Ru nanoparticles due to the extensive formation of Li_2SO_4 was responsible for the loss of the promoting effect of Li with respect to the reference RuA catalyst. For temperatures above 280 °C, the catalytic CO_2 methanation was significantly inhibited, most probably due to the poisoning effect of sulfur directly affecting Ru sites. Even if the bulk decomposition of Li_2SO_4 under H_2 was shown to start only at T>450 °C (Fig. S5), the formation of inactive superficial RuS_x can proceed at lower temperatures: the release of small amounts of H_2S during the last methanation cycles performed at 280 °C over the saturated S-Li-RuA sample (Figs. 8c and S2) strongly supports this argument. As further proof, at the end of the first methanation test over the S-aged DFM, we lowered the temperature back to 200 °C under inert

flow, and we performed a second run on the same sample ("reduced S-Li-RuA" in Fig. 2). A further significant loss of methanation activity was recorded: in particular, up to ca 280 °C the residual reaction rate was reduced by a factor ca 7, while the apparent activation energy was unchanged; moreover, the selectivity to CH_4 remained below 80%. Once again, when the temperature exceeded the threshold level of 280 °C, an additional detrimental effect on the reaction rate and selectivity was observed, which indicates the further self-poisoning of residual Ru sites transformed into inactive RuS_x species. It can be concluded that the remarkable S-tolerance of the Li-RuA DFM comes from a peculiar self-regeneration mechanism active during the CO_2 capture and methanation cycles. Sulfide-covered Ru nanoparticles sites, potentially formed during the hydrogenation step, can be easily reoxidized to RuO_x and SO_2 (but not to sulfates (Kuzmenko et al., 2019)) upon exposure to the oxygen in the flue-gas. Thereafter, RuO_x is quickly reduced back to its active metal form as soon as the DFM is exposed again to hydrogen during the subsequent methanation stage.

Notably, the high intrinsic catalytic activity of the Li-RuA DFM allows to optimally operate the process at temperatures as low as 260–280 °C, thus minimizing the potential self-poisoning effect of sulfur by preventing the formation of any RuS_x, because the catalytic assisted decomposition of Li-sulfates on the DFM is generally negligible below 280–290 °C.

4. Conclusions

Ruthenium (ca 1% wt.) and then Lithium (3% wt.) were sequentially and uniformly dispersed inside γ-Al_2O_3 spherical particles by impregnation with nitrate precursors to obtain a DFM for the integrated CO_2 capture and methanation process. The Li-aluminate phase formed upon reduction at 450 °C favourably interacts with the (10 nm sized) Ru nanoparticles promoting the intrinsic catalytic activity for the methanation of CO_2 well above the reference undoped Ru catalyst.

The DFM showed highly repeatable performances across several cycles of alternated CO_2 capture and methanation in the temperature range 260–320 °C. When both oxygen and water were present in the simulated flue gas a maximum CH_4 production of 250 μmol/g was achieved at ca 260–280 °C, i.e. only 5% below the results obtained under ideal capture conditions (CO_2 in dry N_2). While further improvements of the specific CH_4 productivity are possible by increasing the Li loading, the Li-RuA outperformed by ca 35% a similar Na-RuA DFM with identical metal and alkali loadings.

Eventually, we performed a prolonged ageing study of the DFM under challenging feed conditions with a simulated flue gas containing 10–100 ppmv SO_2 in addition to H_2O and O_2. The Li-RuA DFM showed a remarkable sulfur tolerance during the cyclic operation at 280 °C preserving constant CO_2 conversion and CO selectivity. The DFM completely removed SO_2 storing it as lithium sulfate, which was stable during the subsequent hydrogenation stage, thus avoiding any severe poisoning of the catalytic Ru sites. However, the accumulation of sulfates progressively lowered the CO_2 capture capacity, and, in turn, the CH_4 production, due to the saturation of the Li adsorption sites, which were not regenerated. The removal efficiency for SO_2 approached a breakthrough condition at ca 800 $\mu mol_{SO2}/g_{DFM}$: small quantities of H_2S from sulfate reduction were detected during the methanation stage over the highly sulfated DFM.

Post-ageing characterization of the sulfurized DFM, after more than 100 cycles during 50 days at reaction temperatures, indicated a high stability of its textural properties and a limited increase of the average size of Ru nanoparticles due to sintering. Accordingly, the residual intrinsic methanation activity of the S-aged Li-Ru/A was comparable to the fresh unpromoted Ru catalyst. A clear self-poisoning effect was observed for hydrogenation temperatures beyond 280–290 °C, which is attributed to the formation of RuS_x species by reaction of Li-sulfates with nearby Ru nanoparticles. Nevertheless, exposure of the sulfurized DFM to oxidizing conditions such as those naturally encountered during the CO_2 capture stage can easily decompose inactive RuS_x species, by this way self-regenerating the original catalytic activity for the following methanation stage.

Funding

This research did not receive any specific grant from funding agencies in the public, commercial, or not-for-profit sectors.

Declaration of Competing Interest

The authors declare that they have no known competing financial interests or personal relationships that could have appeared to influence the work reported in this paper.

Supplementary materials

Supplementary material associated with this article can be found, in the online version, at doi:10.1016/j.ccst.2022.100096.

References

Abdallah, M., Farrauto, R., 2022. A perspective on bridging academic research and advanced testing on a path towards pilot plant implementation: a case study of integrating CO_2 capture and catalytic conversion with dual function materials. Catal. Today doi:10.1016/j.cattod.2022.10.005.

Arellano-Treviño, M.A., He, Z., Libby, M.C., Farrauto, R.J., 2019. Catalysts and adsorbents for CO_2 capture and conversion with dual function materials: Limitations of Ni-containing DFMs for flue gas applications. J. CO2 Util. 31, 143–151. doi:10.1016/j.jcou.2019.03.009.

Argyle, M., Bartholomew, C., 2015. Heterogeneous catalyst deactivation and regeneration: a review. Catalysts 5, 145–269. doi:10.3390/catal5010145.

Bermejo-López, A., Pereda-Ayo, B., González-Marcos, J.A., González-Velasco, J.R., 2019. Mechanism of the CO_2 storage and in situ hydrogenation to CH_4. Temperature and adsorbent loading effects over Ru-CaO/Al_2O_3 and Ru-Na_2CO_3/ Al_2O_3 catalysts. Appl. Catal. B Environ. 256, 117845. doi:10.1016/J.APCATB.2019.117845.

Bermejo-López, A., Pereda-Ayo, B., Onrubia-Calvo, J.A., González-Marcos, J.A., González-Velasco, J.R., 2022. Aging studies on dual function materials Ru/Ni-Na/Ca-Al_2O_3 for CO_2 adsorption and hydrogenation to CH4. J. Environ. Chem. Eng. 10, 107951. doi:10.1016/j.jece.2022.107951.

Bermejo-López, A., Pereda-Ayo, B., Onrubia-Calvo, J.A., González-Marcos, J.A., González-Velasco, J.R., 2023. How the presence of O_2 and NO_x influences the alternate cycles of CO_2 adsorption and hydrogenation to CH_4 on Ru-Na-Ca/Al_2O_3 dual function material. J. CO2 Util. 67, 102343. doi:10.1016/J.JCOU.2022.102343.

Cargnello, M., Doan-Nguyen, V.V.T., Gordon, T.R., Diaz, R.E., Stach, E.A., Gorte, R.J., Fornasiero, P., Murray, C.B., 2013. Control of metal nanocrystal size reveals metal-support interface role for ceria catalysts. Science 341 (80), 771–773. doi:10.1126/science.1240148.

Chen, J., Xu, Y., Liao, P., Wang, H., Zhou, H., 2022. Recent progress in integrated CO_2 capture and conversion process using dual function materials: a state-of-the-art review. Carbon Capture Sci. Technol. 4, 100052. doi:10.1016/j.ccst.2022.100052.

Chin, S.Y., Alexeev, O.S., Amiridis, M.D., 2005. Preferential oxidation of CO under excess H_2 conditions over Ru catalysts. Appl. Catal. A Gen. 286, 157–166. doi:10.1016/j.apcata.2005.02.031.

Cimino, S., Torbati, R., Lisi, L., Russo, G., 2009. Sulphur inhibition on the catalytic partial oxidation of methane over Rh-based monolith catalysts. Appl. Catal. A Gen. 360, 43–49. doi:10.1016/j.apcata.2009.02.045.

Cimino, S., Boccia, F., Lisi, L., 2020. Effect of alkali promoters (Li, Na, K) on the performance of Ru/Al_2O_3 catalysts for CO_2 capture and hydrogenation to methane. J. CO2 Util. 37, 195–203. doi:10.1016/j.jcou.2019.12.010.

Cimino, S., Russo, R., Lisi, L., 2022. Insights into the cyclic CO_2 capture and catalytic methanation over highly performing Li-Ru/Al_2O_3 dual function materials. Chem. Eng. J. 428, 131275. doi:10.1016/j.cej.2021.131275.

Cimino, S., Cepollaro, E.M., Lisi, L., 2022. Sulfur tolerance and self-regeneration mechanism of Na-Ru/Al_2O_3 dual function material during the cyclic CO_2 capture and catalytic methanation. Appl. Catal. B Environ. 317, 121705. doi:10.1016/j.apcatb.2022.121705.

Corro, G., Montiel, R., Vázquez, L.C., 2002. Promoting and inhibiting effect of SO_2 on propane oxidation over Pt/Al_2O_3. Catal. Commun. 3, 533–539. doi:10.1016/S1566-7367(02)00210-8.

Das, A.K., De Wilde, J., Heynderickx, G.J., Marin, G.B., Iversen, S.B., Felsvang, K., 2001. Simultaneous adsorption of SO_2 - NOx from flue gases in a riser configuration. AIChE J. 47, 2831–2844. doi:10.1002/aic.690471220.

Du, H., Williams, C.T., Ebner, A.D., Ritter, J.A., 2010. *In situ* FTIR spectroscopic analysis of carbonate transformations during adsorption and desorption of CO_2 in K-Promoted HTlc. Chem. Mater. 22, 3519–3526. doi:10.1021/cm100703e.

Duyar, M.S., Treviño, M.A.A., Farrauto, R.J., 2015. Dual function materials for CO_2 capture and conversion using renewable H2. Appl. Catal. B Environ. 168–169, 370–376. doi:10.1016/j.apcatb.2014.12.025.

Duyar, M.S., Wang, S., Arellano-Treviño, M.A., Farrauto, R.J., 2016. CO utilization with a novel dual function material (DFM) for capture and catalytic conversion to synthetic natural gas: an update. J. CO2 Util. 15, 65–71. doi:10.1016/j.jcou.2016.05.003.

European Commission, Directorate-General for Communication, (2021). European green deal: delivering on our targets, Publications Office of the European Union. https://data.europa.eu/doi/10.2775/373022.

Jeong-Potter, C., Porta, A., Matarrese, R., Visconti, C.G., Lietti, L., Farrauto, R., 2022. Aging study of low Ru loading dual function materials (DFM) for combined power plant effluent CO_2 capture and methanation. Appl. Catal. B Environ. 310, 121294. doi:10.1016/j.apcatb.2022.121294.

Jeong-Potter, C., Abdallah, M., Sanderson, C., Goldman, M., Gupta, R., Farrauto, R., 2022. Dual function materials (Ru+Na_2O/Al_2O_3) for direct air capture of CO_2 and in situ catalytic methanation: the impact of realistic ambient conditions. Appl. Catal. B Environ. 307, 120990.

Kosaka, F., Liu, Y., Chen, S.Y., Mochizuki, T., Takagi, H., Urakawa, A., Kuramoto, K., 2021. Enhanced activity of integrated CO_2 capture and reduction to CH4 under pressurized conditions toward atmospheric CO_2 utilization. ACS Sustain. Chem. Eng. 9, 3452–3463. doi:10.1021/acssuschemeng.0c07162.

Kosaka, F., Sasayama, T., Liu, Y., Chen, S., Mochizuki, T., Matsuoka, K., Urakawa, A., Kuramoto, K., 2022. Direct and continuous conversion of flue gas CO_2 into green fuels using dual function materials in a circulating fluidized bed system. Chem. Eng. J. 450, 138055. doi:10.1016/j.cej.2022.138055.

Kuzmenko, D., Nachtegaal, M., Copéret, C., Schildhauer, T.J., 2019. Molecular-level understanding of support effects on the regenerability of Ru-based catalysts in the sulfur-poisoned methanation reaction. J. Catal. 375, 74–80. doi:10.1016/j.jcat.2019.04.019.

Melo Bravo, P., Debecker, D.P., 2019. Combining CO_2 capture and catalytic conversion to methane. Waste Dispos. Sustain. Energy 1, 53–65. doi:10.1007/s42768-019-00004-0.

Merkouri, L.P., Reina, T.R., Duyar, M.S., 2021. Closing the carbon cycle with dual function materials. Energy Fuels doi:10.1021/acs.energyfuels.1c02729.

Montanari, T., Castoldi, L., Lietti, L., Busca, G., 2011. Basic catalysis and catalysis assisted by basicity: FT-IR and TPD characterization of potassium-doped alumina. Appl. Catal. A Gen. 400, 61–69. doi:10.1016/j.apcata.2011.04.016.

Narayanan, S., Uma, K., 1987. Influence of lithium on reduction, dispersion and hydrogenation activity of nickel on alumina catalysts. J. Chem. Soc. Faraday Trans. 1 Phys. Chem. Condens. Phases. 83, 733–742. doi:10.1039/F19878300733.

Omodolor, I.S., Otor, H.O., Andonegui, J.A., Allen, B.J., Alba-Rubio, A.C., 2020. Dual-function materials for CO_2 capture and conversion: a review. Ind. Eng. Chem. Res. 59, 17612–17631. doi:10.1021/acs.iecr.0c02218.

Porta, A., Falbo, L., Visconti, C.G., Lietti, L., Bassano, C., Deiana, P., 2020. Synthesis of Ru-based catalysts for CO_2 methanation and experimental assessment of intraporous transport limitations. Catal. Today. 343, 38–47. doi:10.1016/j.cattod.2019.01.042.

Porta, A., Matarrese, R., Visconti, C.G., Castoldi, L., Lietti, L., 2021. Storage material effects on the performance of Ru-based CO_2 capture and methanation dual functioning materials. Ind. Eng. Chem. Res. 60, 6706–6718. doi:10.1021/acs.iecr.0c05898.

Porta, A., Visconti, C.G., Castoldi, L., Matarrese, R., Jeong-Potter, C., Farrauto, R., Lietti, L., 2021. Ru-Ba synergistic effect in dual functioning materials for cyclic CO_2 capture and methanation. Appl. Catal. B Environ. 283, 119654. doi:10.1016/j.apcatb.2020.119654.

Povar, I., Spinu, O., 2016. Ruthenium redox equilibria 1. Thermodynamic stability of ru(iii) and ru(iv) hydroxides. J. Electrochem. Sci. Eng. 6, 123–133.

Rönsch, S., Schneider, J., Matthischke, S., Schlüter, M., Götz, M., Lefebvre, J., Prabhakaran, P., Bajohr, S., 2015. Review on methanation – From fundamentals to current projects. Fuel 166, 276–296. doi:10.1016/j.fuel.2015.10.111.

Rege, S.U., Yang, R.T., 2001. A novel FTIR method for studying mixed gas adsorption at low concentrations: H_2O and CO_2 on NaX zeolite and γ-alumina. Chem. Eng. Sci. 56, 3781–3796. doi:10.1016/S0009-2509(01)00095-1.

Saeidi, S., Najari, S., Hessel, V., Wilson, K., Keil, F.J., Concepción, P., Suib, S.L., Rodrigues, A.E., 2021. Recent advances in CO_2 hydrogenation to value-added products — Current challenges and future directions. Prog. Energy Combust. Sci. 85, 100905. doi:10.1016/j.pecs.2021.100905.

Shao, B., Zhang, Y., Sun, Z., Li, J., Gao, Z., Xie, Z., Hu, J., Liu, H., 2022. CO_2 capture and in-situ conversion: recent progresses and perspectives. Green Chem. Eng. 3, 189–198. doi:10.1016/j.gce.2021.11.009.

Sun, S., Lv, Z., Qiao, Y., Qin, C., Xu, S., Wu, C., 2021. Integrated CO_2 capture and utilization with CaO-alone for high purity syngas production. Carbon Capture Sci. Technol. 1, 100001. doi:10.1016/J.CCST.2021.100001.

Sun, S., Sun, H., Williams, P.T., Wu, C., 2021. Recent advances in integrated CO_2 capture and utilization: a review. Sustain. Energy Fuels. 5, 4546–4559. doi:10.1039/d1se00797a.

Sun, Z., Shao, B., Zhang, Y., Gao, Z., Wang, M., Liu, H., Hu, J., 2023. Integrated CO_2 capture and methanation from the intermediate-temperature flue gas on dual functional hybrids of AMS/CaMgO||NiCo. Sep. Purif. Technol. 307, 122680.

Waqif, M., Saad, A.M., Bensitel, M., Bachelier, J., Saur, O., Lavalley, J.C., 1992. Comparative study of SO_2 adsorption on metal oxides. J. Chem. Soc. Faraday Trans. 88, 2931–2936. doi:10.1039/FT9928802931.